

Review

## **Piezoelectric Micromachined Ultrasound Transducer (PMUT) Arrays for Integrated Sensing, Actuation and Imaging**

**Yongqiang Qiu**<sup>1,†</sup>, **James V. Gigliotti**<sup>2,3,†</sup>, **Margeaux Wallace**<sup>2</sup>, **Flavio Griggio**<sup>2,4</sup>,  
**Christine E. M. Demore**<sup>1</sup>, **Sandy Cochran**<sup>1,\*</sup> and **Susan Trolier-McKinstry**<sup>2</sup>

<sup>1</sup> Institute for Medical Science and Technology, University of Dundee, Dundee DD2 1FD, UK;  
E-Mails: y.qiu@dundee.ac.uk (Y.Q.); c.demore@dundee.ac.uk (C.E.M.D.)

<sup>2</sup> Materials Research Institute, The Pennsylvania State University, University Park, PA 16802, USA;  
E-Mails: jamey.gigliotti@gmail.com (J.V.G.); margeaux.wallace@gmail.com (M.W.);  
flavio.griggio@gmail.com (F.M.); stmckinstry@psu.edu (S.T.-M.)

<sup>3</sup> Materials Science and Engineering, Georgia Institute of Technology, Atlanta, GA 30332-0245, USA

<sup>4</sup> Intel Corporation, Hillsboro, OR 97124, USA

† These authors contributed equally to this work.

\* Author to whom correspondence should be addressed; E-Mail: s.cochran@dundee.ac.uk;  
Tel.: +44-1382-386-991; Fax: +44-1382-386-588.

Academic Editor: Xiaoning Jiang

Received: 13 February 2015 / Accepted: 26 March 2015 / Published: 3 April 2015

---

**Abstract:** Many applications of ultrasound for sensing, actuation and imaging require miniaturized and low power transducers and transducer arrays integrated with electronic systems. Piezoelectric micromachined ultrasound transducers (PMUTs), diaphragm-like thin film flexural transducers typically formed on silicon substrates, are a potential solution for integrated transducer arrays. This paper presents an overview of the current development status of PMUTs and a discussion of their suitability for miniaturized and integrated devices. The thin film piezoelectric materials required to functionalize these devices are discussed, followed by the microfabrication techniques used to create PMUT elements and the constraints the fabrication imposes on device design. Approaches for electrical interconnection and integration with on-chip electronics are discussed. Electrical and acoustic measurements from fabricated PMUT arrays with up to 320 diaphragm elements are presented. The PMUTs are shown to be broadband devices with an operating frequency which is tunable by tailoring the lateral dimensions of the flexural membrane or the thicknesses of the constituent layers. Finally, the outlook for future development of

PMUT technology and the potential applications made feasible by integrated PMUT devices are discussed.

**Keywords:** ultrasound; piezoelectric thin films; micromachined ultrasound transducers; arrays; integrated transducers

## 1. Introduction

In the last several decades, ultrasound has found ever-expanding industrial and biomedical applications, such as non-destructive evaluation (NDE) [1,2], ultrasonic actuation [3], medical imaging [4,5], therapeutic ultrasound [6], and particle and cell manipulation [7,8], at frequencies from tens of kilohertz to hundreds of megahertz. Ultrasound can be excited by many different methods, including the piezoelectric effect, magnetostriction, and the photoacoustic effect [9,10]. Of these, the piezoelectric effect is the most common. A typical structure of a conventional piezoelectric ultrasonic transducer is shown in Figure 1a. It usually has a layer of piezoelectric material sandwiched by thin high conductivity electrode layers, of e.g., Au or Pt, often with an underlying adhesion layer e.g., of Cr or Ti, and connected with electrical wires.

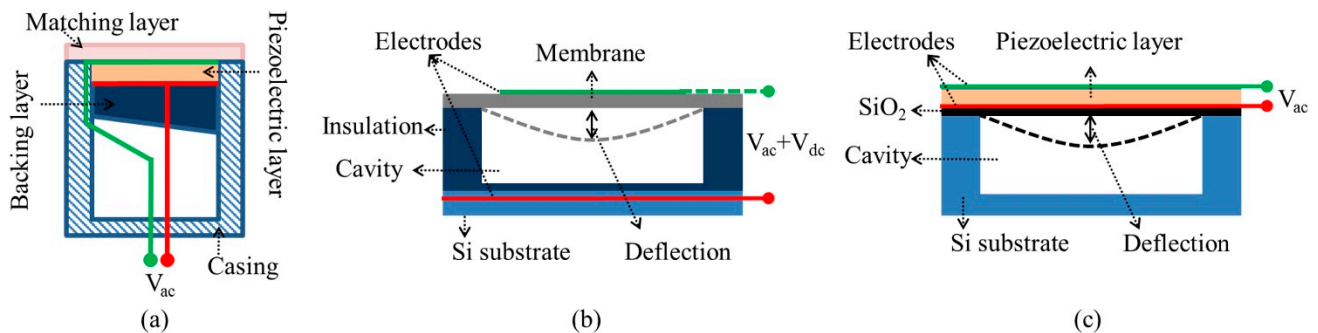


**Figure 1.** Typical cross-sectional structures of (a) piezoelectric ultrasonic transducers; (b) CMUTs and (c)  $d_{31}$ -mode PMUTs.

For this kind of transducer, the longitudinal vibration mode ( $d_{33}$ -mode) of the piezoelectric material is utilized. Thus the anti-resonant frequency of the transducer is related to the thickness of the piezoelectric layer and the longitudinal velocity of sound in the poling direction of the piezoelectric material [11]. This direct dependence of the resonant frequency on the layer thickness therefore limits the transducer geometry and structure for specific applications. For example, the resonant frequency of a thin film of lead zirconate titanate (PZT) in the  $d_{33}$ -mode is at least several hundreds of megahertz. This ultrahigh frequency may benefit ultrasound microbeam cell manipulation [12]. However, the high attenuation associated with this frequency range limits the penetration depth of ultrasound in tissue and thus it is very rarely used in ultrasound imaging applications. In addition, acoustic impedance ( $Z_{ac}$ ) mismatching between the piezoelectric layer ( $Z_{ac} > 30$  MRayl for conventional PZT) and the load medium, e.g., air ( $\sim 400$  Rayl), water ( $\sim 1.5$  MRayl) or soft tissue ( $\sim 1.6$  MRayl) [13], can limit the energy transmission and reduce the bandwidth, even with matching layers placed on the front face of

the piezoelectric material. This also ignores the manufacturing difficulty and complexity of matching layers with precise thickness for high frequency ultrasound transducers [10,14,15]. Furthermore, the fabrication difficulty of conventional piezoelectric transducer structures increases dramatically for 1-D linear and 2-D matrix ultrasound arrays for beam steering and 3-D volumetric imaging [5,16], and in miniaturized devices with high element density to be fitted into small, constrained spaces, e.g., in intravascular ultrasound (IVUS) and intracardiac echocardiography (ICE) catheters [17–19].

Many of these problems can potentially be overcome by micromachined ultrasound transducers (MUTs). The MUT family includes capacitive micromachined ultrasonic transducers (CMUTs) based on the flexural vibrations caused by a field-induced electrostatic attraction between suspended membrane and the substrate (Figure 1b) [20–25], and piezoelectric micromachined ultrasonic transducers (PMUTs) based on flexural vibrations caused by  $d_{31}$ - [26–38] or  $d_{33}$ -mode [39–41] excitation of a piezoelectric membrane (Figure 1c).

A CMUT element is, in essence, a miniaturized capacitor that consists of a thin metallized suspended membrane, e.g., silicon nitride ( $\text{Si}_x\text{N}_y$ ), over a cavity with a rigid metallized substrate, e.g., silicon (Si), as shown in Figure 1b. When a DC voltage is applied between the two electrodes, the membrane is deflected, being attracted toward the substrate by electrostatic forces. The mechanical restoring force caused by the stiffness of the membrane resists the attraction [25]. Consequently, ultrasound can be generated from the oscillations of the membrane with an AC voltage input.

In contrast, the deflection of the membrane in the PMUT is caused by the lateral strain generated from the piezoelectric effect of the membrane, which must thus include at least one piezoelectric layer, typically a thin  $\text{PbZr}_{1-x}\text{Ti}_x\text{O}_3$ , PZT, film [30,42], as well as a passive elastic layer. In this case, the resonant frequency of the PMUT does not directly depend on the thickness of the piezoelectric layer. Instead, the flexural mode resonant frequencies are closely related to the shape, dimensions, boundary conditions, intrinsic stress and mechanical stiffness of membranes, as they are also in CMUTs.

Intrinsic stress in the membrane generated during fabrication can affect the resonant frequency dramatically. In the case of an edge-clamped circular diaphragm with low intrinsic stress, the membrane behaves as a plate with the resonant frequencies,  $f$ , given as [43–45]:

$$f = \frac{\alpha}{2\pi r^2} \sqrt{\frac{D_E}{\rho h}} \quad (1)$$

$$D_E = \frac{Eh^3}{12(1-\nu^2)} \quad (2)$$

where  $\alpha$  is the resonance mode constant,  $r$  is the radius of the diaphragm,  $D_E$  is the flexural rigidity,  $\rho$  is the effective density of the diaphragm,  $h$  is the diaphragm thickness,  $E$  is the effective Young's modulus, and  $\nu$  is Poisson's ratio. With high intrinsic stress,  $T$ , the stress can dominate over the flexural rigidity, hence the membrane behaves as a membrane with no bending stiffness with the resonant frequencies given as [43–45]:

$$f = \frac{\alpha}{2\pi r} \sqrt{\frac{T}{\rho h}} \quad (3)$$

Therefore, the resonant frequency of the MUTs can be controlled with proper selection of the radius of the diaphragm with tailored effective mechanical stiffness, leading to better design flexibility regardless of any thickness restrictions of the piezoelectric layer. Since the bandwidth may be narrow in some designs, it is also possible to arrange a set of MUTs with different diaphragm sizes and frequencies to broaden the bandwidth and improve upon the sensitivity of a single device [34]. A soft membrane with tuneable  $Z_{ac}$  leads to better impedance matching with the load media, thus theoretically improving the energy transmission and bandwidth [24]. Through wafer-scale microfabrication [46], miniaturized transducer arrays with high element density can be fabricated to meet the functional and geometrical requirements of new applications [21,35]. Microfabrication techniques also give the possibility to integrate MUTs with circuitry and front-end electronics in the same chip [21,24].

CMUTs have been demonstrated to produce high bandwidths (up to 175%) and electromechanical coupling coefficients ( $\sim 0.85$ ) and output acoustic pressure exceeding conventional transducers [20,23,24,47]. However, in practice, the high performance can only be achieved when a large DC bias near the so-called collapse voltage is applied, which increases the risk of failure of the device. This can, to some extent, limit performance in biomedical applications. Although new driving methods have been demonstrated [48], the problem remains. Moreover, different CMUT designs may be required for transmission and reception because of different cavity height requirements; thus, different transmission and reception arrays may be required for imaging applications [30].

Unlike CMUTs, PMUTs do not require a large voltage bias and have fewer geometric and design constraints, facilitating integration with low voltage electronics. PMUTs also offer several other advantages over CMUTs, largely because of their higher capacitance and lower electrical impedance. These increase the transducer sensitivity by decreasing the effects of parasitic capacitance while enabling use of low voltage electronics [30,32,49,50]. Large output signals, low loss and high signal-to-noise ratios (SNR) can be further achieved with the implementation of piezoelectric thin films [37,42,51]. Although printed thick film piezoelectric materials can lead to low cost devices, it is usually with a loss of performance. Furthermore, challenges remain for integrated electronics and fine-scale interconnects for miniaturized devices [52].

Despite the promise of PMUTs, the high sensitivity of the resonant frequency to the residual stress of the membrane may cause difficulties during the design process [34,49,53–55]. Also, it is essential to locate the neutral axis outside the piezoelectric layer to maximize the net polarization change in the receive mode [29]. Therefore, the metallized piezoelectric layer is usually deposited on passive elastic layers such as Si,  $\text{Si}_x\text{N}_y$  or  $\text{SiO}_2$ . The optimal layer thicknesses and configuration identified from modelling can ensure maximum sensitivity of the piezoelectric layer and allow for better tuning of the mechanical stiffness of the membrane.

To date, several research groups have successfully developed PMUTs with different fabrication approaches and achieved promising results. Most PMUTs are fabricated using similar techniques, with altered processes mainly dependent on the chosen substrates and thin film piezoelectric materials. This paper presents an overview of recent advances towards the development of miniaturized and integrated arrays with PMUT technology, including a review of a specific new process. In the following sections, the requirements of the piezoelectric materials and variety of possible fabrication methods for PMUT elements and arrays are discussed.

## 2. Piezoelectric Materials for PMUTs

As is the case for conventional ultrasound transducers, the piezoelectric material most widely used in PMUTs is PZT, a ferroelectric material first formulated in the 1950s by Jaffe [56]. Although other materials (e.g., PVDF [57,58], AlN [59,60] and ZnO [27,61–64]) have been relatively commonly reported in PMUTs, especially in early devices, these usually have a weaker piezoelectric response than ferroelectric oxide films (including PZNT [34,65]). PZT-based compositions are therefore better for low voltage actuation and high sensitivity sensing [42,66].

PZT thin films usually have a thickness between a few nanometers and  $\sim 3 \mu\text{m}$ . In order to deposit material with good ferroelectric properties on a silicon substrate, buffer layers are required to prevent lead diffusion and oxidation reactions [66]. As bottom electrodes are needed for most applications, electrodes such as platinum [35] and SrRuO<sub>3</sub> [67] may act as one of the buffer layers. A number of coating methods have been adapted for the deposition of PZT thin films, including physical methods such as ion beam sputtering, RF magnetron sputtering, and pulsed-laser deposition (PLD), and chemical methods such as sol-gel deposition, metal-organic-decomposition (MOD) and metal-organic-chemical vapor deposition (MOCVD) [66]. Both sputtering [36,68] and sol-gel deposition [26,28,32,37,69–71] methods have often been used to prepare PZT thin films with large piezoelectric coefficients and high remanent polarization for use in PMUTs.

As an example, Figure 2 shows a 1  $\mu\text{m}$  thick PZT film sputtered on a Pt/Ti/SiO<sub>2</sub>/Si wafer with an RF sputtering system (CMS-18, Kurt J. Lesker Co., Jefferson Hills, PA, USA). The results of X-ray diffraction (XRD) and the hysteresis loop of the PZT thin film suggest a high quality was achieved.

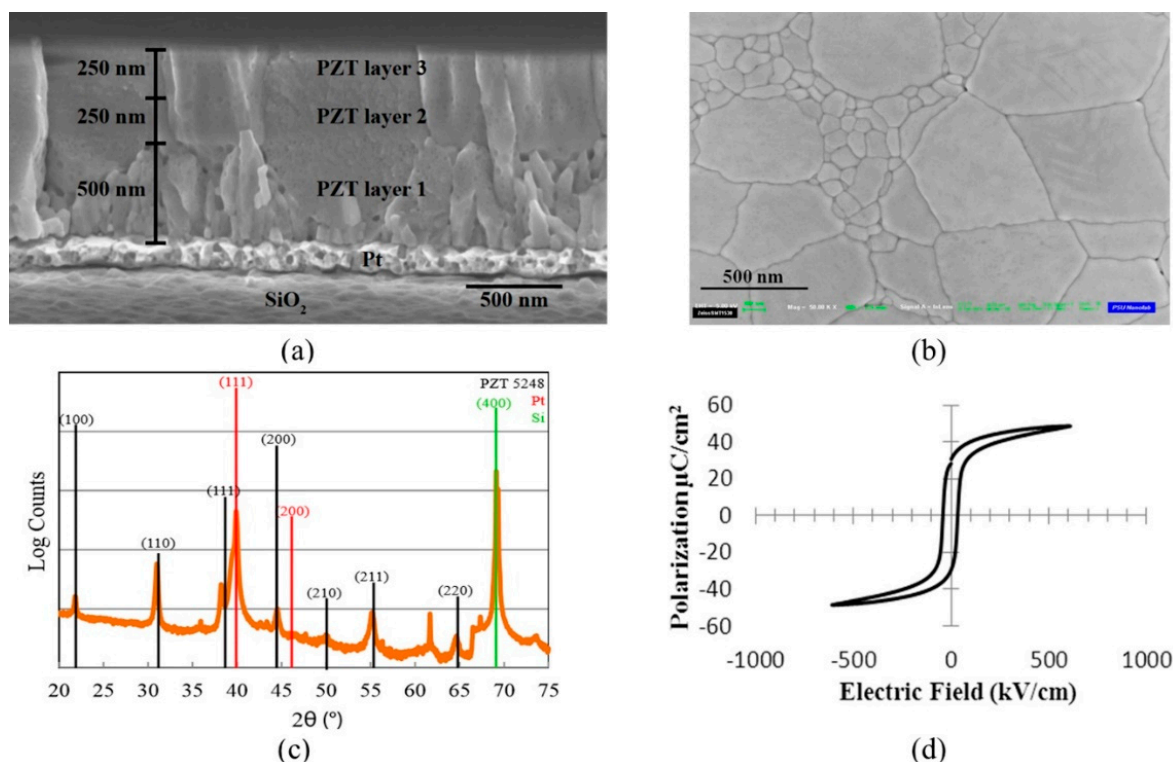


**Figure 2.** FESEM images of (a) cross-sectional and (b) top surface of PZT thin film; (c) XRD pattern of the PZT film with the absence of PbO ( $2\theta = 29.09^\circ$ ) and pyrochlore/fluorite ( $2\theta = 29.55^\circ$ ); (d) hysteresis loop of the sputtered PZT thin film.

The effective piezoelectric response of PZT thin films is usually very different from that of bulk PZT, particularly because of the in-plane clamping of the film by the substrate, as well as from the residual stress in the film [42]. By releasing the substrate beneath the thin film PZT, the mechanical constraints near the bottom interface of the PZT are reduced and the piezoelectric domain walls can more freely respond to the electric field and contribute more to the dielectric and piezoelectric properties, leading to better performance of the PMUTs [36,72]. Partially unclamping diaphragm edges [32,60,73], optimizing electrode configurations [55,74,75] and even adding DC bias [33,76,77] have also been used to increase the coupling coefficients and acoustic output of PMUTs.

### 3. Fabrication of PMUT Element

#### 3.1. Diaphragm Defined with Sacrificial Layer Releasing

A sacrificial layer release process has been used frequently for microfabrication of both CMUTs [20,22,24,25] and PMUTs [27,62,78]. This usually involves initial sacrificial layer preparation on the substrate. After completing fabrication and patterning of all layers of the diaphragm, it is then released by etching the sacrificial layer through a small opening to form a cavity below the diaphragm. Perçin *et al.* demonstrated the fabrication of ZnO-based PMUT arrays with a low temperature oxide (LTO) as the sacrificial layer [27]. The process is shown in Figure 3.

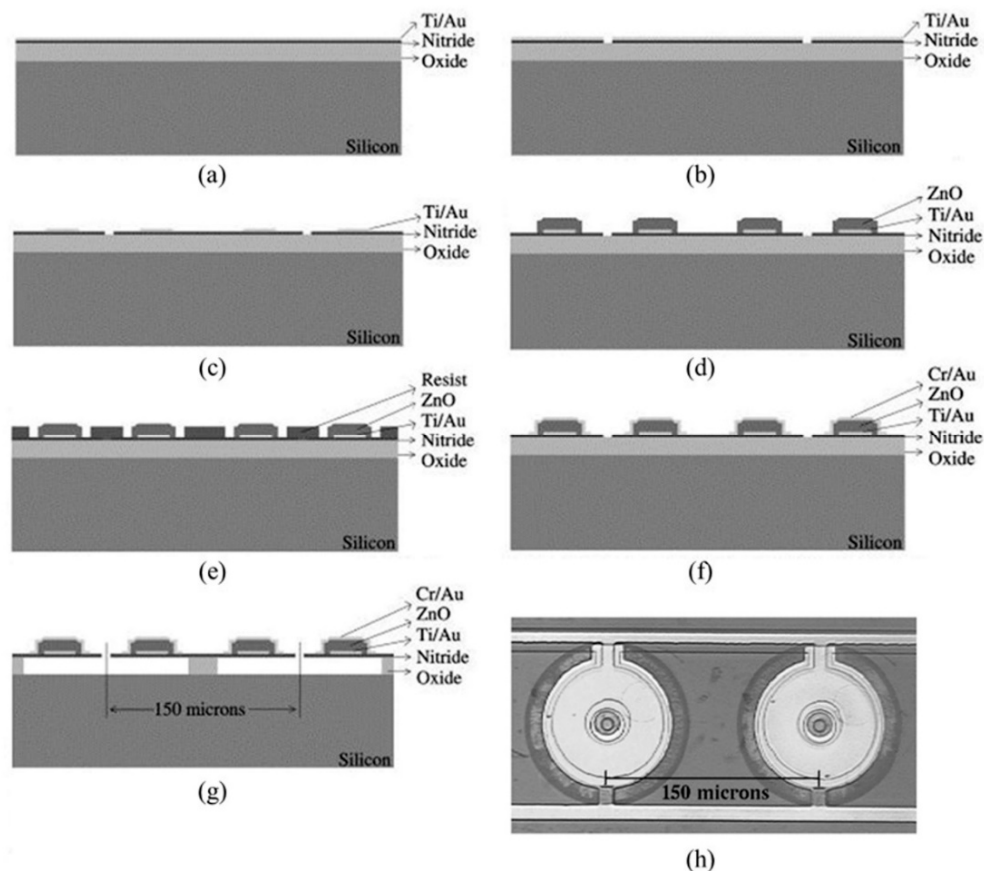


**Figure 3.** (a–g) Typical sacrificial layer release process flow; and (h) top view of two fabricated adjacent PMUT elements. © 1998 AIP Publishing LLC. Reprinted with permission from [27].

First, a layer of 8% phosphorus-doped densified LTO was prepared on a Si substrate, followed by a thin layer of silicon nitride ( $\text{Si}_3\text{N}_4$ ) deposited by low-pressure chemical vapor deposition (LPCVD) and a bottom Ti/Au electrode layer deposited by e-beam evaporation (Figure 3a).  $\text{Ø}8 \mu\text{m}$  access holes for releasing the final diaphragms were then defined by wet etching of the electrode layer and plasma etching of  $\text{Si}_3\text{N}_4$  (Figure 3b). After patterning the bottom electrode layer (Figure 3c), a  $0.3 \mu\text{m}$  thick layer of ZnO was sputtered on top of the bottom electrode and patterned into ring shapes with inner and outer diameters of  $30 \mu\text{m}$  and  $80 \mu\text{m}$  respectively by wet etching (Figure 3d). The top Cr/Au electrode layer was deposited by e-beam evaporation and patterned by a lift-off process (Figure 3e,f). Finally, the LTO sacrificial layer was wet etched (Figure 3g). A top view of two adjacent elements of the fabricated PMUT is shown in Figure 3h.

ZnO was used in this process but other thin film piezoelectric materials such as PZT can also be adopted. However, limitations still exist regarding the lateral etching rate of the sacrificial layer and the compatibility of the membrane stack with the etching processes for the sacrificial layers [46]. Therefore, many recent PMUTs have been developed with other processes for diaphragm formation.

### 3.2. Diaphragm Defined with Back-Side Etching

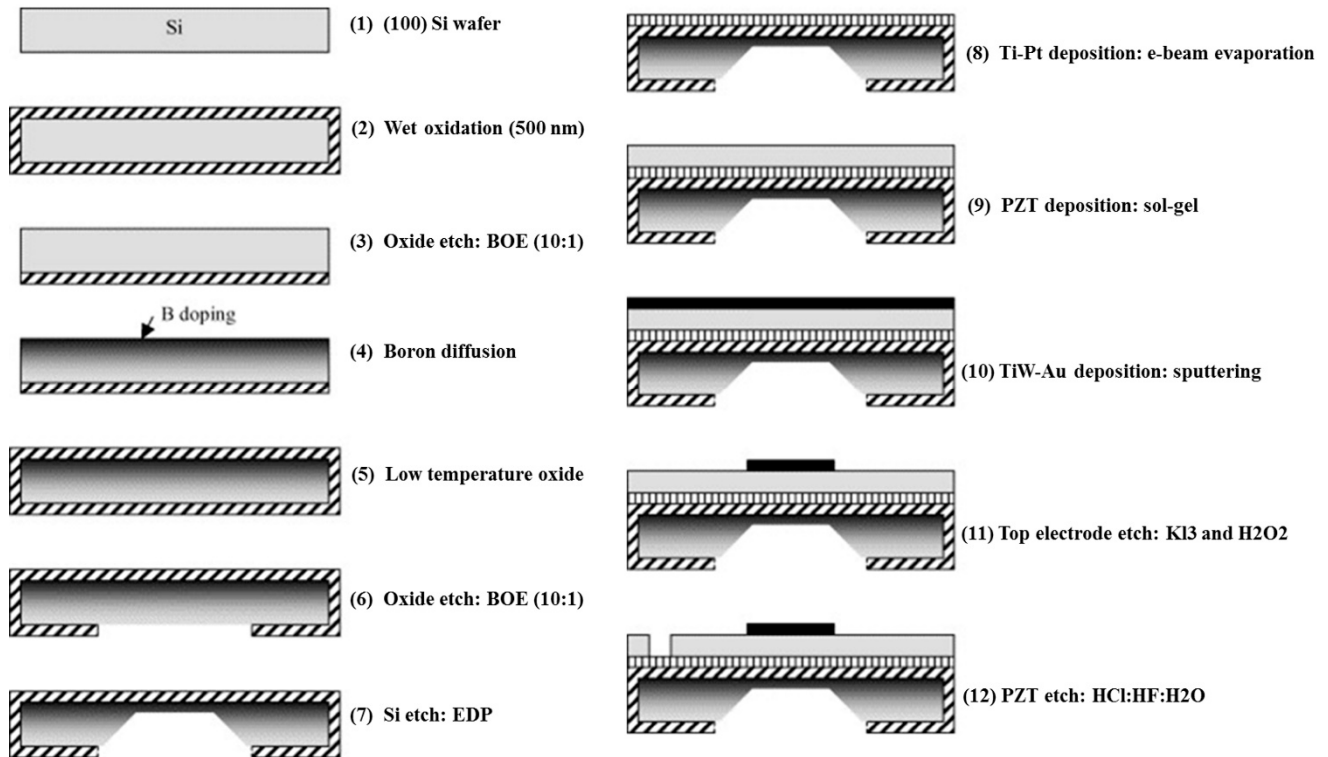
An alternative is to define the diaphragm with back-side etching. The etching step itself can take place either before deposition of the piezoelectric layer [28,30,64,79–81] or after completing the whole membrane stack [26,31,52]. Small variations in the design of these two processes are mainly due to the initial substrates and different etch stops. In many early devices, a boron-doped Si layer was used as the etch-stop layer [26,30,57]. Alternatively, silicon on insulator (SOI) wafers can be employed with a tailored thickness of the device layer, with the buried oxide layer then used as an etch stop [28,32,33,69,70,73,75].

Figure 4 shows a fabrication process flow starting with a (100) Si wafer [30]. As is the case for surface micromachining, the process begins with preparation of the insulator (e.g.,  $\text{SiO}_2$  or  $\text{Si}_3\text{N}_4$ ) on the silicon. This is then etched from one side of the Si in preparation for B doping. B diffusion occurs at a specific rate, allowing control of the junction depth. After doping, the surface is cleaned then coated with LTO.

Subsequently, standard photolithography is used to pattern the back-side etch window. Later, the wafer is etched with an etchant such as ethylenediamine-pyrocatechol-water-pyrazine (EDP). After the back-side etching, a Ti/Pt bottom electrode is deposited by e-beam evaporation, followed by deposition of PZT and the top electrode. Finally, the top electrode and PZT are etched separately to pattern the top electrode and access the bottom electrode.

In this process, EDP is used as the etchant, but other anisotropic wet etchants can also be used, e.g., potassium hydroxide (KOH) [31,52,82] and tetramethylammonium hydroxide (TMAH) [46,83], depending on the etch stops and the requirement of etch rate selectivity.





**Figure 4.** Fabrication process flow of PMUT element with diaphragm defined by back-side etching © 2004 Elsevier B.V. Reprinted with permission from [30].

One of the disadvantages of the anisotropic etching in this process is the creation of  $54.7^\circ$  sloping sidewalls [30], as shown in Figure 5. This limits the minimum size of diaphragm and the pitch of the transducer array the process can create. In turn, this constrains the maximum frequency of the transducer array that can be obtained because, ideally, a half-wavelength ( $\lambda/2$ ) pitch is required to avoid grating lobe effects in ultrasound imaging applications. Therefore, the back-side etching in current devices is usually performed with deep reactive-ion etching (DRIE), obtaining relatively perpendicular side walls [32,33,35,59,60,64,70], and this works well with SOI wafers using the buried oxide as the etch stop [32,33,70].

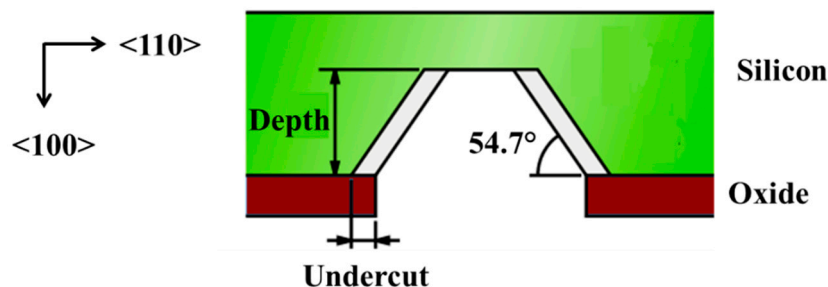


**Figure 5.** Sloping sidewalls are formed with anisotropic wet etching.

### 3.3. Diaphragm Defined with Front-Side Etching

An alternative route to define the diaphragm cavity is to etch the Si substrate through the membrane from the front (surface micromachining) [36,67]. Figure 6 shows a fabrication process flow for



PMUTs with circular diaphragms released from the front-side. Here, the underlying Si substrate was isotropically etched through predefined etch vias. The final membrane of the fabricated PMUTs comprised a SiO<sub>2</sub>/Ti/Pt/PZT/Pt polymer stack.

A 1 µm thick layer of PZT was grown on a commercial platinized Si wafer by RF sputter deposition at room temperature. The wafer had 1 µm thick thermal SiO<sub>2</sub>, 20 nm of Ti and 150 nm of (111) oriented Pt, and was thermally cleaned prior to the deposition. To avoid film cracking and improve density, the film was grown in three successive layers of thicknesses 500 nm, 250 nm and 250 nm, annealed in O<sub>2</sub> after each growth, as seen in Figure 2. Then a layer of Pt was sputtered on the PZT as the top electrode and annealed at 500 °C to improve adhesion. The top electrode was patterned via contact lithography and RIE. The access to the bottom Ti/Pt electrode was achieved by reactive ion etching (RIE) of the exposed PZT using a thick photoresist mask.

Later, before the fabrication of the electrode fan-out, a layer of SiO<sub>2</sub> was prepared as an insulation pad on the exposed PZT by sputter deposition and lift-off, reducing potential parasitic capacitance associated with the electrode fan-out and bond pads. Ti/Pt was then sputtered and patterned via lift-off to create a conformal connection to the top electrode of the PZT. Etch vias were created to access the bare silicon beneath the stack to allow for front-side release of the diaphragms. The stack of Pt, PZT, Ti/Pt and SiO<sub>2</sub> was etched with RIE.

To allow multiple diameters of diaphragms and to avoid damaging the fragile membranes after release, the wafer was diced prior to further steps. Immediately prior to release, any native oxide on the bare Si was removed with a brief CF<sub>4</sub> etch to ensure symmetrical cavities. The diaphragms were then defined with XeF<sub>2</sub> isotropic etching. Depending on the number of XeF<sub>2</sub> etching cycles, different diameters can be obtained. A Ø35 µm hemispheric cavity is shown in Figure 6b.

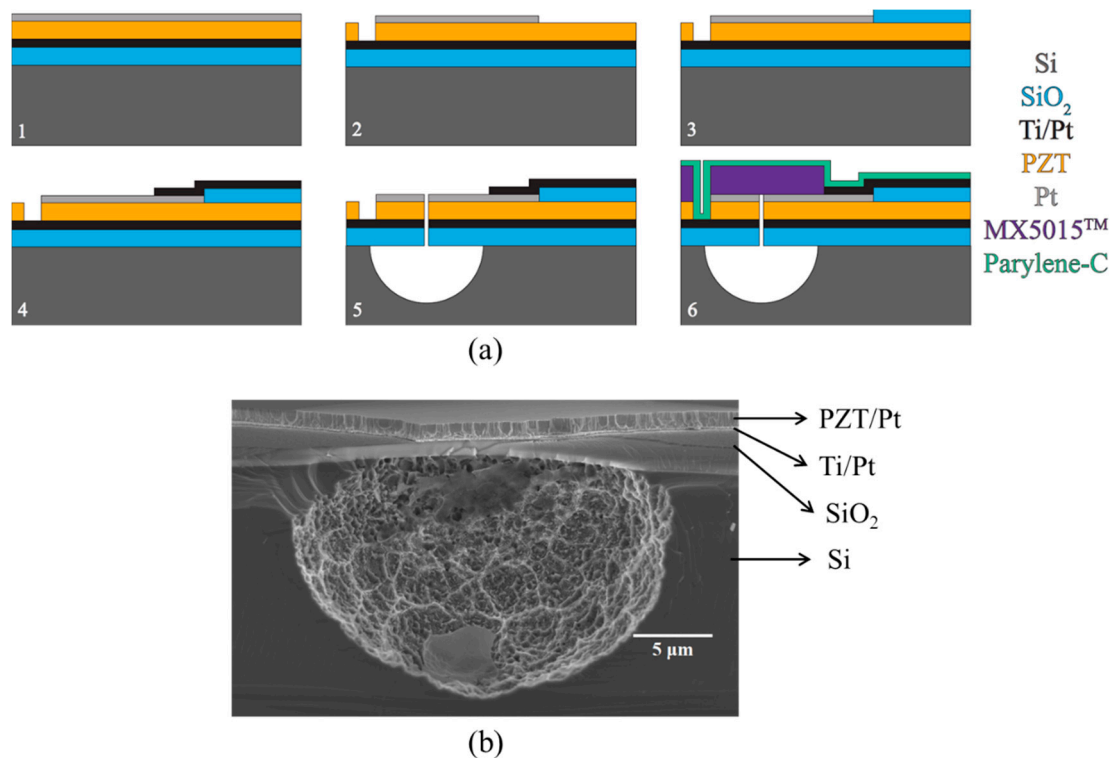


**Figure 6.** (a) Fabrication process flow of PMUTs with diaphragm defined by front-side etching; (b) FESEM cross-sectional image of a released cavity.

To prevent backfill of the etch cavity and improve acoustic performance, the diaphragms were laminated with a 15  $\mu\text{m}$  thick negative photoresist film (MX5015, DuPont Electronic Technologies, Hertfordshire, UK) to seal the vias. Prior to lamination, the dies were cleaned with an  $\text{O}_2$  plasma to improve laminate adhesion. The laminate was then patterned to expose the bond pads for wire bonding. After wire bonding, the complete packages were cleaned with an Ar plasma then coated with parylene. To improve the hydrophilicity of the parylene, the surface was activated in an  $\text{O}_2$  plasma for several seconds.

The advantage of this front-side release process is that cavities of relatively smaller diameter can be achieved easily. As mentioned earlier, the necessary element pitch of high frequency transducer arrays imposes limits on the size of PMUT cavities, e.g., diameter  $<50 \mu\text{m}$  for frequency  $>30 \text{ MHz}$ . However, an additional layer must be added to the device after diaphragm fabrication to seal the etch vias through the membrane. This layer in turn increases the effective stiffness of the membrane, increasing the resonant frequency of the PMUTs.

### 3.4. Wafer Transfer Diaphragm Formation

Another approach to diaphragm formation is to fabricate the cavity and the PMUT membrane independently on two substrates and bond the two parts together [71,79,84,85].

Figure 7 shows the fabrication process flow for PMUTs with diaphragms formed by such a bonding process [71]. First,  $\text{SiO}_2$  and  $\text{Si}_3\text{N}_4$  are grown on a Si substrate. After patterning, high-density cavities and air channel structures are etched on one side of the substrate, e.g., using KOH.

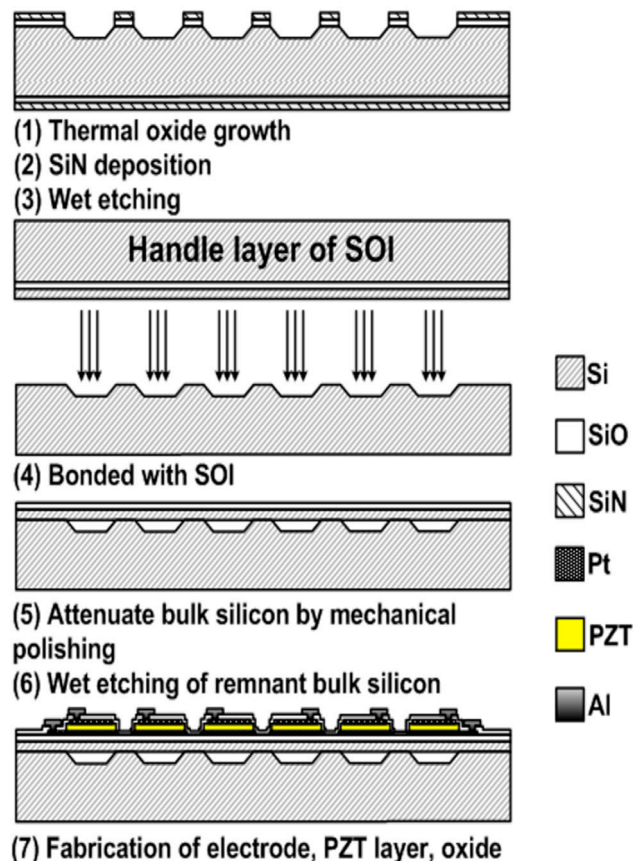


**Figure 7.** Fabrication process flow of PMUTs with diaphragms formed by reverse bonding [71].

The air channel structures are used for compensation of the air pressure in the sealed cavities, preventing potential damage of the membrane stack during annealing. Subsequently, a SOI wafer is bonded on top of the Si substrate with the cavities at atmospheric pressure. The device layer of SOI is left as the supporting structure for the cavities. Then the handle layer of SOI is removed by chemical mechanical polishing (CMP) and wet etching processes to expose the buried oxide layer.

The bottom electrode (Ti/Pt), PZT and top electrode layers are deposited and patterned subsequently on the buried oxide layer with the Ti/Pt electrode also acting as a barrier layer to prevent inter-diffusion between PZT and SiO<sub>2</sub>. Then a thin layer of SiO<sub>2</sub> is deposited by PECVD to protect the top electrode and PZT during the fabrication of the Al electrode fan-out and bond pads. This completes the PMUTs with a membrane stack of Si/SiO<sub>2</sub>/Ti/Pt/PZT/Pt suspended above the cavities as shown in Figure 8.

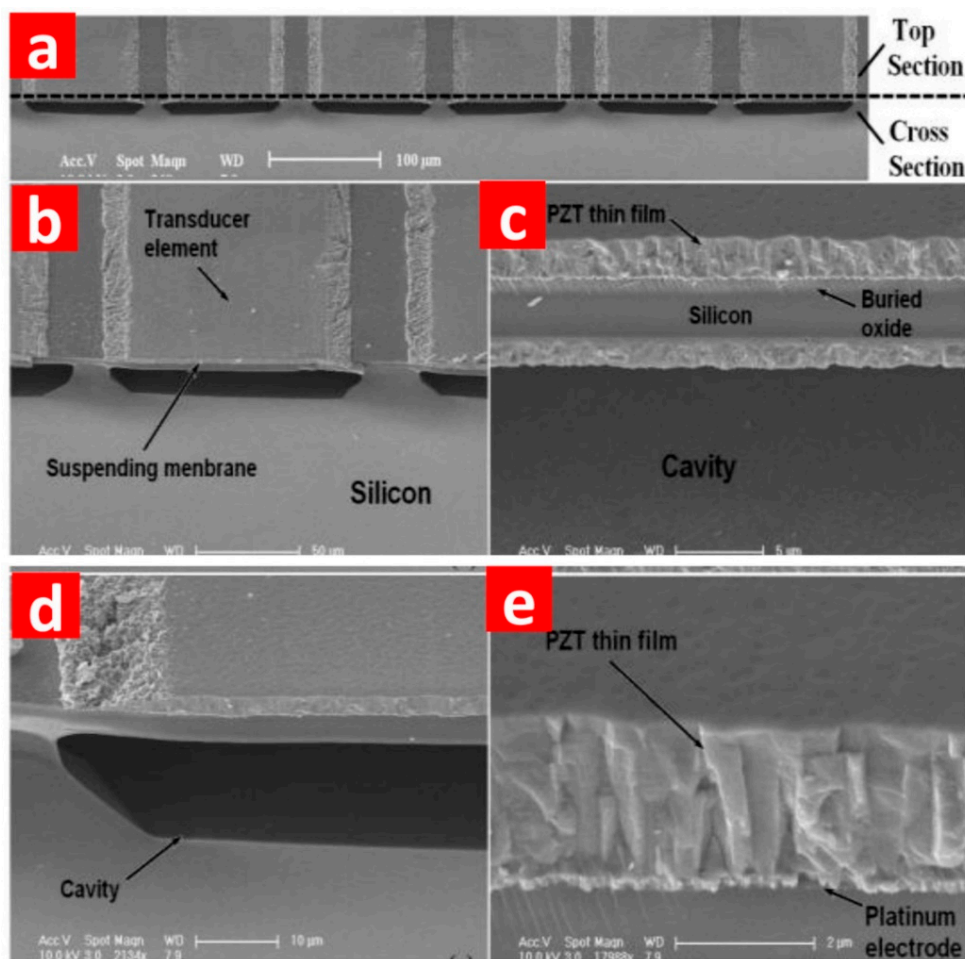


**Figure 8.** SEM images of (a) oblique view of the structure of PMUTs; (b) oblique view of a single PMUT element; (c) the suspended membrane stack; (d) oblique view of the cavity; and (e) the PZT thin film layer [71].

In this process, the practical size of the PMUT element is defined by the initial cavity etching. Thus the main constraint on the interspace between two adjacent PMUT elements is the accuracy of lithography and the alignment through the whole process [71,79,84,85].

#### 4. Development of PMUT Arrays

Generally, a transducer with a single element cannot fully satisfy many practical applications, especially in medical imaging and NDE. Instead, the use of multiple transducer elements and dynamic control of each element is used to achieve electronic beam steering, focusing and scanning, which bring benefits in reduction of test time and better reliability and quality of measurements.

Linear arrays, Figure 9, have a number of transducer elements arranged in a line. Each element usually has the same geometrical shape with width in the lateral direction and height in the elevation direction. The distance between the centers of two adjacent elements is defined as the pitch, and the gap between them is the kerf. The pitch is often smaller than  $\lambda$ , ideally  $\lambda/2$ , to avoid grating lobe effects which will degrade the image quality. In the operation of a linear array, only a subset of elements is activated each time to transmit or receive, and a scan is realized by altering the selection of active elements, as shown in Figure 9a. The ultrasound beam is transmitted perpendicular to the element surface, giving a smaller activated aperture than the whole transducer. If a phase delay is introduced into the signal applied to each element of the linear array, ultrasound beam focusing and steering can be achieved, as shown in Figure 9b. Linear arrays with phase delay control in which all the elements of the array are active as one set are called phased linear arrays.

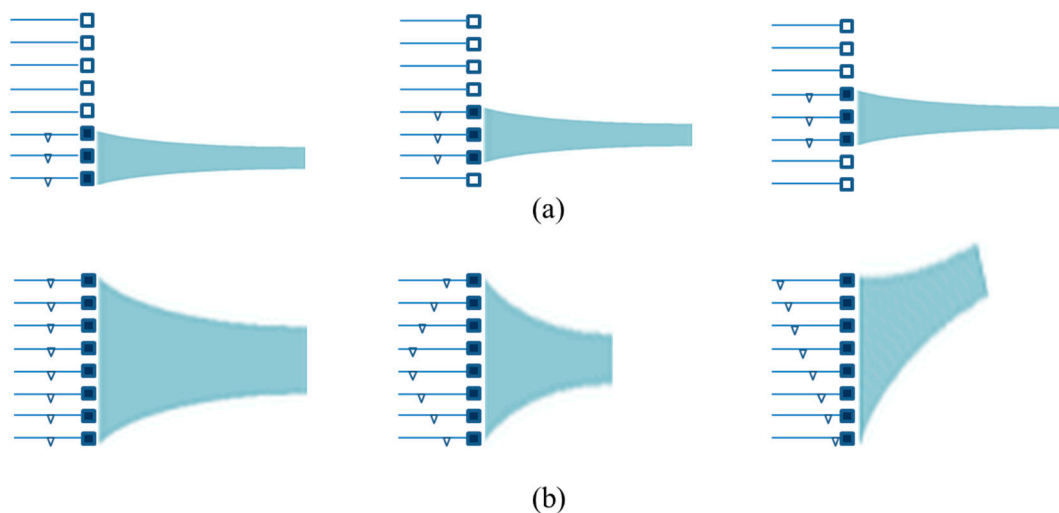


**Figure 9.** Schematic diagrams of (a) electronic scanning of 1-D linear arrays; (b) electronic focusing and steering of 1-D phased linear arrays.

For 1-D linear PMUT arrays, each array element is usually formed by connecting multiple PMUT elements in parallel and driving them together. Figure 10 shows 32-element PMUT arrays fabricated by the authors for high frequency applications through the fabrication process detailed in Section 3.3. Each PMUT array element consisted of ten  $\text{Ø}80 \mu\text{m}$  PMUT elements with shared electrodes.

To test the 32-element PMUT arrays, a conventional un-matched PZT piezocomposite transducer of 30.5 MHz center frequency and 36%  $-6$  dB fractional bandwidth [86] was used, first with the PMUT operating as a receiver, with the piezocomposite transducer transmitting, then with the PMUT operating as a transmitter, with the piezocomposite receiving. Because the  $-6$  dB ultrasound beam diameter of the piezocomposite transducer was about  $80 \mu\text{m}$  at the focal point, thus the beam was incident principally only on one or two diaphragms in the PMUT array element.



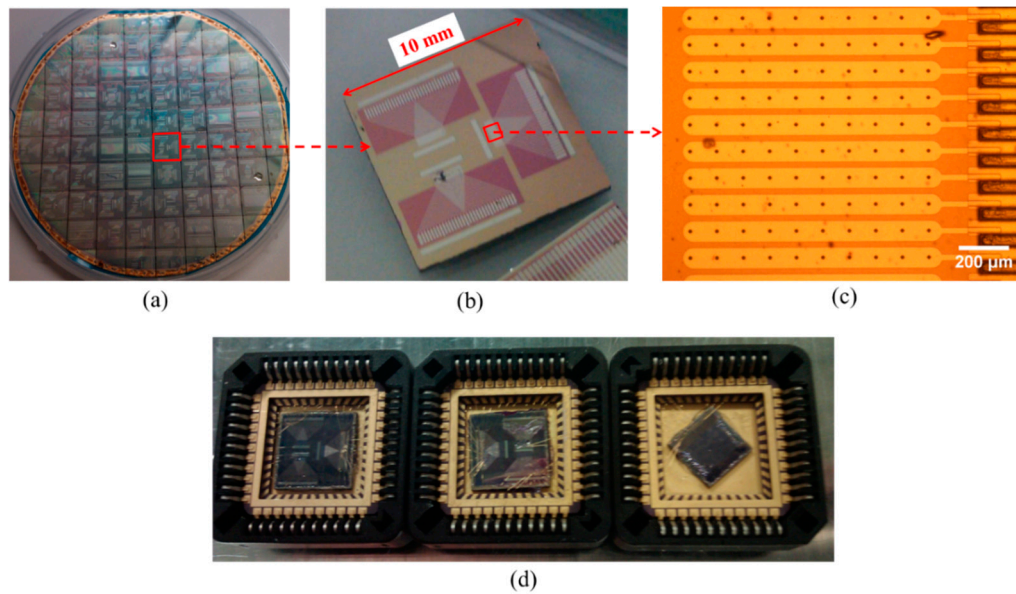


**Figure 10.** Images of (a) a 4-inch wafer with multiple PMUT dies with different diameter diaphragms; (b) three PMUT arrays on one die; (c) several elements of a PMUT array, each consisting of ten diaphragms; and (d) three fully packaged wire-bonded devices.

Therefore, a five degree-of-freedom platform was used to fine tune the alignment of the transmitter and the receiver, *i.e.*, orientation and position, in order to achieve better SNR and to maximize the signal amplitude of the received pulse. The distance between the transmitter and the receiver was close to the focal length of the piezocomposite transducer,  $\sim 4$  mm. The acoustic response of the PMUT array shown in Figure 11, on both reception and transmission, demonstrates the achievement of reasonable sensitivity and relatively large bandwidth.

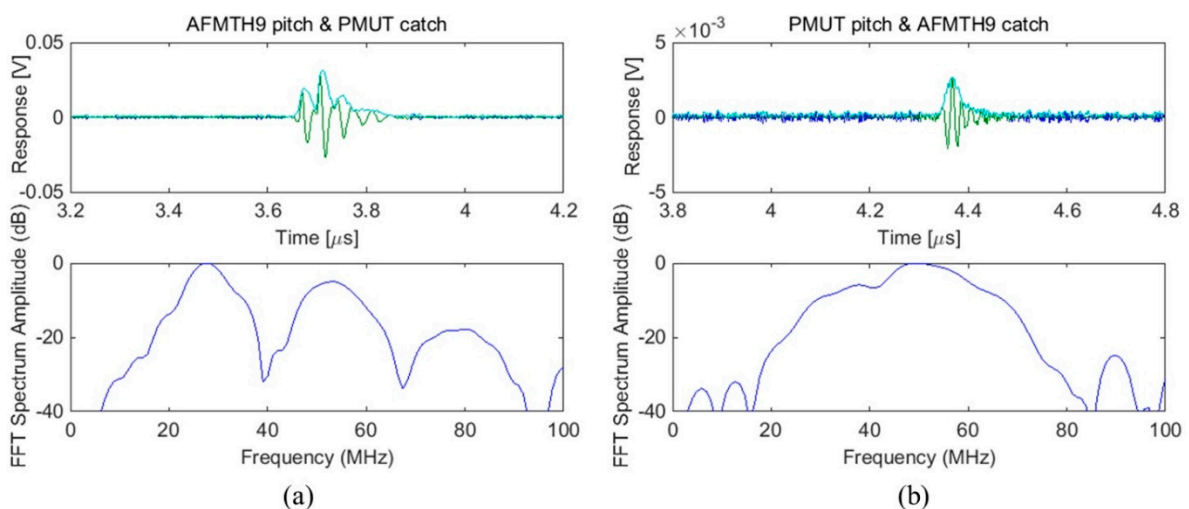


**Figure 11.** (a) Receive and (b) transmit response of one element in a PMUT array measured with a 30.5 MHz piezocomposite transducer in deionized water. In the time-domain figures, the blue curve represents original signal with green part of Tukey-windowed signal, and the cyan curve represents Hilbert transformed signal; in the frequency-domain figures, the blue curve represents the FFT spectrum of the Tukey-windowed signal.

It was noticed that the center frequency and  $-6$  dB bandwidths in reception were close to the pulse-echo response of the piezocomposite transducer, but smaller than those in the transmit response. This result was anticipated, because the frequency and bandwidth of the  $\text{Ø}80 \mu\text{m}$  PMUT diaphragms were expected to be greater than those of the un-matched piezocomposite transducer. For lower frequency PMUT arrays, multiple lines of PMUT elements can be integrated into one array element [34], as shown in Figure 12. Moreover, by arranging pre-shaped PMUTs with slightly different diameters, a broader bandwidth and improved sensitivity can be realized through the complex interaction between the individual PMUT elements [34,65].

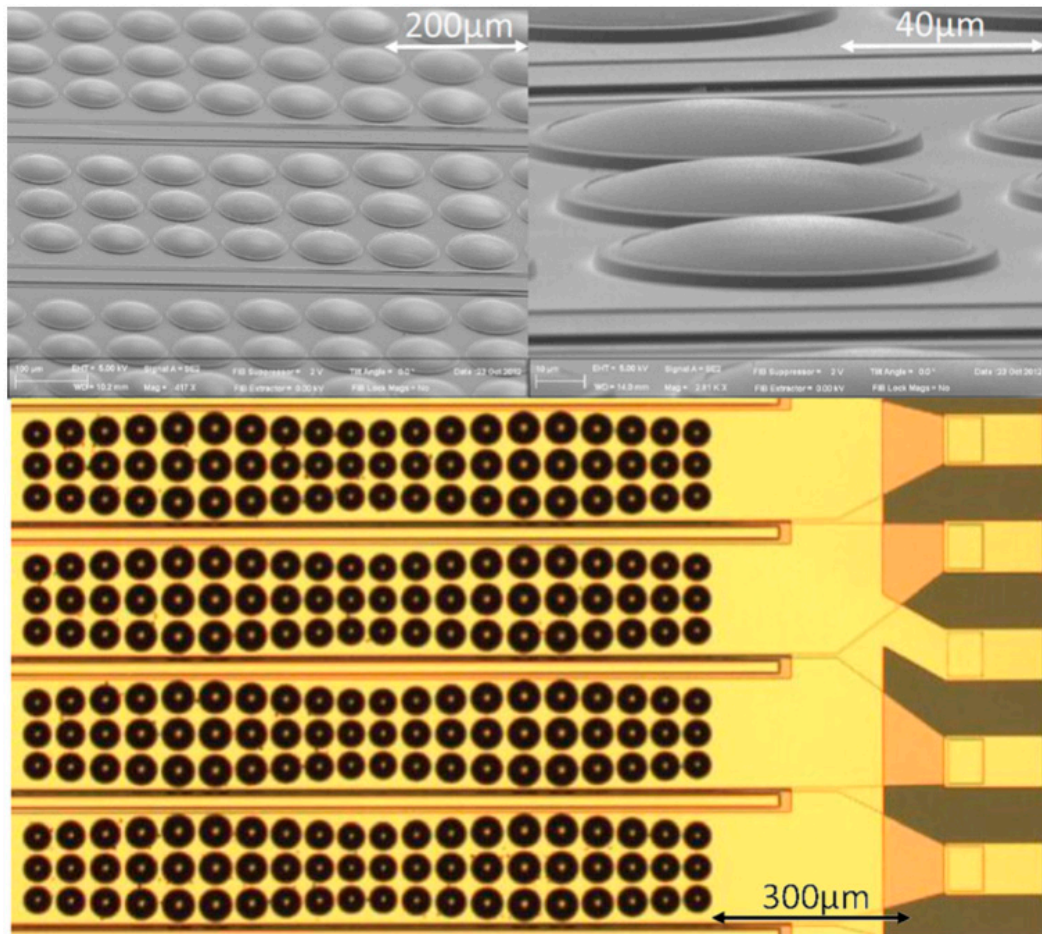


**Figure 12.** SEM and optical images of a 64 channel 5 MHz linear array exploiting five different dome sizes with cavities ranging from  $74$  to  $90 \mu\text{m}$  diameter. © 2012 AIP Publishing LLC. Reprinted with permission from [34].

The principle of 2-D arrays is similar to that of linear arrays, but with multiple elements in the elevation direction so that the beam can be controlled dynamically in two orthogonal directions with appropriate phased delays. Therefore, 2-D arrays usually have a large number of elements forming a matrix. The ultrasound beam can be fully steered in 2-D, allowing maximum electronic control flexibility. However, the electrical interconnection is more difficult than 1-D arrays, as individual electrical addressing is usually required for each element, as shown in Figure 13 [71]. An alternative is to use a crossed-electrode array configuration with row-column addressing [70] to reduce the complexity of interconnects, but control flexibility is also constrained, reducing array performance.

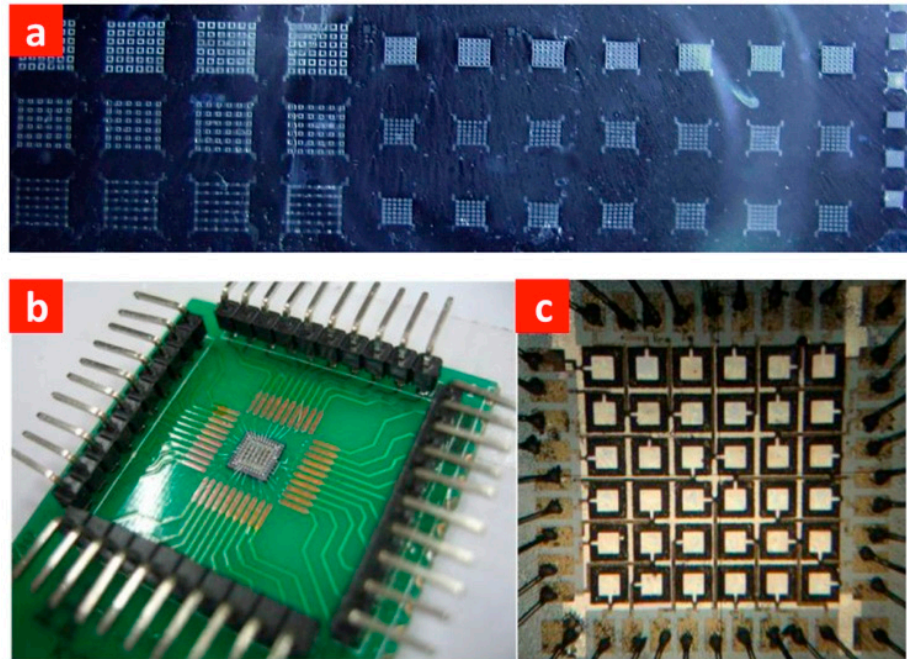


**Figure 13.** Photographs of (a) 2D PMUT arrays; (b) a packaged array used for testing; and (c) a  $6 \times 6$  2-D PMUT matrix array with element size  $200 \mu\text{m} \times 200 \mu\text{m}$  and total area less than  $2 \text{mm} \times 2 \text{mm}$  [71].

More recently, Dausch *et al.* [35] have successfully developed intracardiac echocardiography (ICE) catheters integrated with 5 MHz PMUT matrix arrays of 256 and 512 elements, as shown in Figure 14. Through-Si interconnects were adopted to allow individual addressing of each element in a constrained space. This allowed demonstration of real-time *in vivo* 3-D imaging using a PMUT matrix array integrated device in which the electrodes of the PMUT elements were led to the back surface of the PMUT substrate (Figure 14a), and thermo-compression bonding was used to bond the PMUT substrate onto the wiring substrate with epoxy (Figure 14b). This interconnection scheme not only enables good electrical interconnection to the PMUTs without significantly increasing electronic footprint or using other time-consuming interconnect means (e.g., wire-bonding), but also further reduces the overall dimensions of PMUT array devices [35].

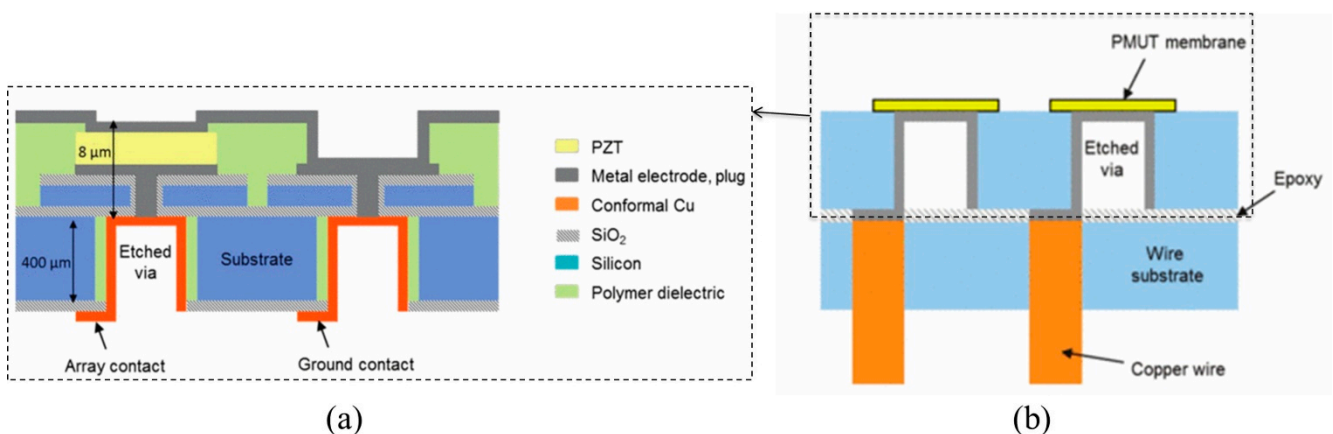


**Figure 14.** *Cont.*



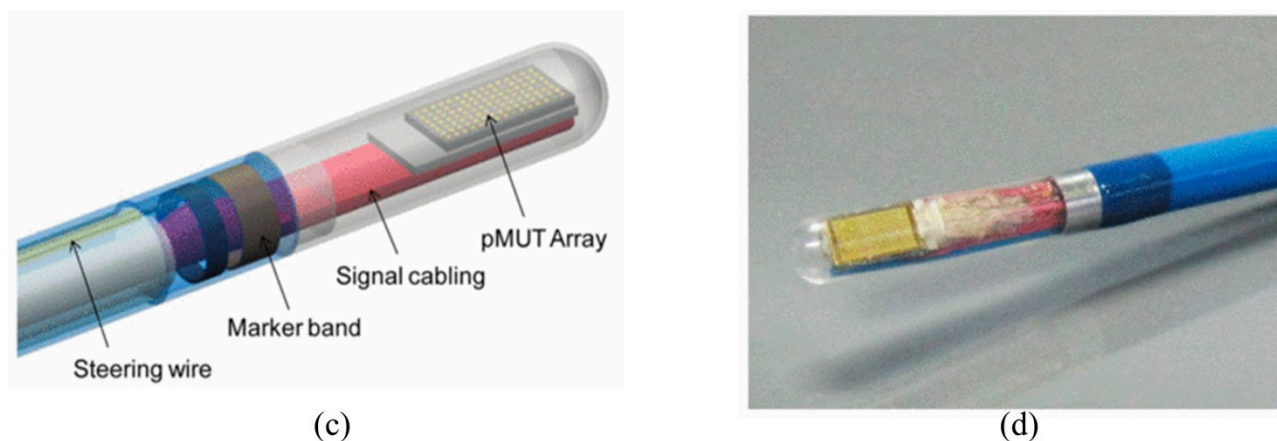


**Figure 14.** Cross-sectional schematic diagrams of (a) PMUTs with through-Si interconnects and (b) a PMUT array substrate bonded onto a wiring substrate; (c) a mechanical model and (d) photograph of the distal end of a steerable 14-Fr ( $\text{\O}4.667$  mm) ICE catheter containing a 512-element PMUT matrix array. © 2013 IEEE. Reprinted with permission from [35].

## 6. Conclusions and Outlook

In recent years, increasing attention has been given to MUTs because of their advantages over conventional ultrasound transducers, such as miniaturization, low  $Z_{ac}$ , high bandwidth and sensitivity, and high electromechanical coupling coefficient, and with potential for automated large batch production and integration with front-end electronics. Both CMUTs and PMUTs have been explored; the latter require deposition of piezoelectric layers but are less limited by geometric and electronic constraints, with reduced power consumption.

Compared to the conventional ultrasound transducers and CMUTs, only a relatively limited number of publications on PMUTs has appeared over the last 25 years, which may be attributed to two reasons: the difficulties in the manufacture of high performance piezoelectric thin films, and the lack of efficient modelling methods or tools for accurate prediction of the effects of intrinsic stress. These challenges have therefore led to developed PMUTs with lower performance in practice than theory. However, substantial progress has been made to improve the performance, with a particular focus on innovative fabrication approaches [34,35,65], device structures [32,34,60,65,70,73] and drive methods [33,34], and better models [34,53,55].

Continuing research in PMUTs will focus on further improvement of interconnect solutions and acoustic performance (e.g., sensitivity and bandwidth), matching the development of other miniaturized devices to address unmet needs in industry and medicine, e.g., in ultrasound capsule endoscopy [87].

## Acknowledgments

The authors thank the Royal Society, London, UK, for an International Exchange grant that supported interaction between their groups at the Pennsylvania State University and the University of Dundee. Some of the device fabrication was funded by a National Security Science and Engineering Faculty Fellowship from the US Office of the Secretary of Defense.

## Conflicts of Interest

The authors declare no conflict of interest.

## References

1. Drinkwater, B.W.; Wilcox, P.D. Ultrasonic arrays for non-destructive evaluation: A review. *NDT E Int.* **2006**, *39*, 525–541.
2. Jiang, X.; Kim, K.; Zhang, S.; Johnson, J.; Salazar, G. High-temperature piezoelectric sensing. *Sensors* **2013**, *14*, 144–169.
3. Watson, B.; Friend, J.; Yeo, L. Piezoelectric ultrasonic micro/milli-scale actuators. *Sens. Actuators A Phys.* **2009**, *152*, 219–233.
4. Donald, I.; Macvicar, J.; Brown, T. Investigation of abdominal masses by pulsed ultrasound. *Lancet* **1958**, *271*, 1188–1195.
5. Fenster, A.; Downey, D.B. 3-D ultrasound imaging: a review. *IEEE Eng. Med. Biol. Mag.* **1996**, *15*, 41–51.
6. Haar, G.R. Ter High Intensity Focused Ultrasound for the Treatment of Tumors. *Echocardiography* **2001**, *18*, 317–322.
7. Qiu, Y.; Wang, H.; Demore, C.E.M.; Hughes, D.A.; Glynne-Jones, P.; Gebhardt, S.; Bolhovitins, A.; Poltarjonoks, R.; Weijer, K.; Schönecker, A.; *et al.* Acoustic devices for particle and cell manipulation and sensing. *Sensors* **2014**, *14*, 14806–14838.
8. Coakley, W.T.; Bardsley, D.W.; Grundy, M.A.; Zamani, F.; Clarke, D.J. Cell manipulation in ultrasonic standing wave fields. *J. Chem. Technol. Biotechnol.* **1989**, *44*, 43–62.
9. Cheeke, J.D.N. *Fundamentals and Applications of Ultrasonic Waves*, 2nd ed.; CRC Press: London, UK, 2012; pp. 1–504.
10. Cochran, S. 1—Piezoelectricity and basic configurations for piezoelectric ultrasonic transducers. In *Ultrasonic Transducers*; Nakamura, K., Ed.; Woodhead Publishing Limited: Cambridge, UK, 2012; pp. 3–35.
11. 176-1987—IEEE Standard on Piezoelectricity. Available online: <http://ieeexplore.ieee.org/xpl/articleDetails.jsp?arnumber=26560&contentType=Standards> (accessed on 3 April 2015).
12. Lee, J.; Lee, C.; Kim, H.H.; Jakob, A.; Lemor, R.; Teh, S.-Y.; Lee, A.; Shung, K.K. Targeted cell immobilization by ultrasound microbeam. *Biotechnol. Bioeng.* **2011**, *108*, 1643–1650.
13. Cobbold, R.S.C. *Foundations of Biomedical Ultrasound*; Biomedical Engineering Series; Oxford University Press: New York, NY, USA, 2006; pp. 1–832.
14. Shung, K.K.; Zipparo, M. Ultrasonic transducers and arrays. *IEEE Eng. Med. Biol. Mag.* **1996**, *15*, 20–30.
15. Brown, J.A.; Sharma, S.; Leadbetter, J.; Cochran, S.; Adamson, R. Mass-Spring Matching Layers for High-Frequency Ultrasound Transducers: A New Technique Using Vacuum Deposition. *IEEE Trans. Ultrason. Ferroelectr. Freq. Control* **2014**, *61*, 1911–1921.
16. Gonçalves, L.F.; Espinoza, J.; Kusanovic, J.P.; Lee, W.; Nien, J.K.; Santolaya-Forgas, J.; Mari, G.; Treadwell, M.C.; Romero, R. Applications of 2-dimensional matrix array for 3- and 4-dimensional examination of the fetus: A pictorial essay. *J. Ultrasound Med.* **2006**, *25*, 745–755.

17. Light, E.; Lieu, V.; Smith, S. New fabrication techniques for ring-array transducers for real-time 3D intravascular ultrasound. *Ultrason. Imaging* **2009**, *31*, 247–256.
18. Wang, Y.; Stephens, D.N.; O'Donnell, M. Optimizing the beam pattern of a forward-viewing ring-annular ultrasound array for intravascular imaging. *IEEE Trans. Ultrason. Ferroelectr. Freq. Control* **2002**, *49*, 1652–1664.
19. Bruce, C.J.; Friedman, P.A. Intracardiac echocardiography. *Eur. J. Echocardiogr.* **2001**, *2*, 234–244.
20. Ladabaum, I.; Jin, X.; Soh, H.T.; Atalar, A.; Khuri-Yakub, B.T. Surface micromachined capacitive ultrasonic transducers. *IEEE Trans. Ultrason. Ferroelectr. Freq. Control* **1998**, *45*, 678–690.
21. Gurun, G.; Tekes, C.; Zahorian, J.; Xu, T.; Satir, S.; Karaman, M.; Hasler, J.; Degertekin, F.L. Single-chip CMUT-on-CMOS front-end system for real-time volumetric IVUS and ICE imaging. *IEEE Trans. Ultrason. Ferroelectr. Freq. Control* **2014**, *61*, 239–250.
22. Park, K.; Oralkan, O.; Khuri-Yakub, B. A comparison between conventional and collapse-mode capacitive micromachined ultrasonic transducers in 10-MHz 1-D arrays. *IEEE Trans. Ultrason. Ferroelectr. Freq. Control* **2013**, *60*, 1245–1255.
23. Soh, H.T.; Ladabaum, I.; Atalar, A.; Quate, C.F.; Khuri-Yakub, B.T. Silicon micromachined ultrasonic immersion transducers. *Appl. Phys. Lett.* **1996**, *69*, 3674.
24. Eccardt, P.C.; Niederer, K. Micromachined ultrasound transducers with improved coupling factors from a CMOS compatible process. *Ultrasonics* **2000**, *38*, 774–780.
25. Khuri-Yakub, B.T.; Oralkan, O. Capacitive micromachined ultrasonic transducers for medical imaging and therapy. *J. Micromech. Microeng.* **2011**, *21*, 54004–54014.
26. Bernstein, J.J.; Finberg, S.L.; Houston, K.; Niles, L.C.; Chen, H.D.; Cross, L.E.; Li, K.K.; Udayakumar, K. Micromachined high frequency ferroelectric sonar transducers. *IEEE Trans. Ultrason. Ferroelectr. Freq. Control* **1997**, *44*, 960–969.
27. Perçin, G.; Atalar, A.; Levent Degertekin, F.; Khuri-Yakub, B.T. Micromachined two-dimensional array piezoelectrically actuated transducers. *Appl. Phys. Lett.* **1998**, *72*, 1397.
28. Yamashita, K.; Katata, H.; Okuyama, M.; Miyoshi, H.; Kato, G.; Aoyagi, S.; Suzuki, Y. Arrayed ultrasonic microsensors with high directivity for in-air use using PZT thin film on silicon diaphragms. *Sens. Actuators A Phys.* **2002**, *97–98*, 302–307.
29. Muralt, P.; Baborowski, J. Micromachined ultrasonic transducers and acoustic sensors based on piezoelectric thin films. *J. Electroceram.* **2004**, *12*, 101–108.
30. Akasheh, F.; Myers, T.; Fraser, J.D.; Bose, S.; Bandyopadhyay, A. Development of piezoelectric micromachined ultrasonic transducers. *Sens. Actuators A Phys.* **2004**, *111*, 275–287.
31. Wang, Z.; Zhu, W.; Tan, O.K.; Chao, C.; Zhu, H.; Miao, J. Ultrasound radiating performances of piezoelectric micromachined ultrasonic transmitter. *Appl. Phys. Lett.* **2005**, *86*, 033508.
32. Muralt, P.; Ledermann, N.; Paborowski, J.; Barzegar, A.; Gentil, S.; Belgacem, B.; Petitgrand, S.; Bosseboeuf, A.; Setter, N. Piezoelectric micromachined ultrasonic transducers based on PZT thin films. *IEEE Trans. Ultrason. Ferroelectr. Freq. Control* **2005**, *52*, 2276–2288.
33. Dausch, D.E.; Castellucci, J.B.; Chou, D.R.; von Ramm, O.T. Theory and operation of 2-D array piezoelectric micromachined ultrasound transducers. *IEEE Trans. Ultrason. Ferroelectr. Freq. Control* **2008**, *55*, 2484–2492.

34. Hajati, A.; Latev, D.; Gardner, D.; Hajati, A.; Imai, D.; Torrey, M.; Schoeppler, M. Three-dimensional micro electromechanical system piezoelectric ultrasound transducer. *Appl. Phys. Lett.* **2012**, *101*, 253101.
35. Dausch, D.E.; Gilchrist, K.H.; Carlson, J.B.; Hall, S.D.; Castellucci, J.B.; von Ramm, O.T. *In vivo* real-time 3-D intracardiac echo using PMUT arrays. *IEEE Trans. Ultrason. Ferroelectr. Freq. Control* **2014**, *61*, 1754–1764.
36. Griggio, F.; Demore, C.E.M.; Kim, H.; Gigliotti, J.; Qiu, Y.; Jackson, T.N.; Tutwiler, R.L.; Cochran, S.; Trolrier-McKinstry, S. Micromachined diaphragm transducers for miniaturised ultrasound arrays. In Proceedings of 2012 IEEE International Ultrasonics Symposium, Dresden, Germany, 7–10 October 2012; pp. 1–4.
37. Hong, E.; Krishnaswamy, S.V.; Freidhoff, C.B.; Trolrier-McKinstry, S. Micromachined piezoelectric diaphragms actuated by ring shaped interdigitated transducer electrodes. *Sens. Actuators A Phys.* **2005**, *119*, 521–527.
38. Hong, E.; Trolrier-McKinstry, S.; Smith, R.; Krishnaswamy, S.V.; Freidhoff, C.B. Vibration of micromachined circular piezoelectric diaphragms. *IEEE Trans. Ultrason. Ferroelectr. Freq. Control* **2006**, *53*, 697–706.
39. Bernstein, J.J.; Bottari, J.; Houston, K.; Kirkos, G.; Miller, R.; Xu, B.; Ye, Y.; Cross, L.E. Advanced MEMS ferroelectric ultrasound 2D arrays. In Proceedings of 1999 IEEE Ultrasonics Symposium, Caesars Tahoe, NV, USA, 17–20 October 1999; Volume 2, pp. 1145–1153.
40. Klee, M.; Mauczok, R.; van Heesch, C.; Boots, H.; de Wild, M.; op het Veld, B.; Soer, W.; Schmitz, G.; Mleczo, M. Piezoelectric thin film platform for ultrasound transducer arrays. In Proceedings of 2011 IEEE International Ultrasonics Symposium, Orlando, FL, USA, 18–21 October 2011; pp. 196–199.
41. Klee, M.; Boots, H.; Kumar, B.; van Heesch, C.; Mauczok, R.; Keur, W.; de Wild, M.; van Esch, H.; Roest, A.L.; Reimann, K.; *et al.* Ferroelectric and piezoelectric thin films and their applications for integrated capacitors, piezoelectric ultrasound transducers and piezoelectric switches. *IOP Conf. Ser. Mater. Sci. Eng.* **2010**, *8*, 012008.
42. Trolrier-McKinstry, S.; Muralt, P. Thin film piezoelectrics for MEMS. *J. Electroceram.* **2004**, *12*, 7–17.
43. Hong, E. Surface Micromachined Peristaltic Pumps Using Lead Zirconate Titanate Film, Ph.D. Thesis, The Pennsylvania State University, State College, PA, USA, 2004; pp. 1–195.
44. Timoshenko, S.P.; Woinowsky-Krieger, S. *Theory of Plates and Shells*; McGraw-Hill: Singapore, 1959; pp. 1–579.
45. Morse, P.M.; Ingard, K.U. *Theoretical Acoustics*; Princeton University Press: Princeton, NJ, USA, 1987; pp. 1–949.
46. Baborowski, J. Microfabrication of piezoelectric MEMS. *J. Electroceram.* **2004**, *12*, 33–51.
47. Ergun, A.S.; Cheng, C.-H.; Oralkan, O.; Johnson, J.; Jagannathan, H.; Demirci, U.; Yaralioglu, G.G.; Karaman, M.; Khuri-Yakub, B.T. Broadband capacitive micromachined ultrasonic transducers ranging from 10 kHz to 60 MHz for imaging arrays and more. In Proceedings of 2002 IEEE Ultrasonics Symposium, Munich, Germany, 8–11 October 2002, pp. 1039–1043.

48. Bayram, B.; Haeggström, E.; Yaralioglu, G.G.; Khuri-Yakub, B.T. A new regime for operating capacitive micromachined ultrasonic transducers. *IEEE Trans. Ultrason. Ferroelectr. Freq. Control* **2003**, *50*, 1184–1190.
49. Akasheh, F.; Fraser, J. Piezoelectric micromachined ultrasonic transducers: Modeling the influence of structural parameters on device performance. *IEEE Trans. Ultrason. Ferroelectr. Freq. Control* **2005**, *52*, 455–468.
50. Vernet, J.L.; Steichen, W.; Lardat, R.; Garcia, O.; Gelly, J.F. PMUTS design optimization for medical probes applications. In Proceedings of 2001 IEEE Ultrasonics Symposium; Atlanta, GA, USA, 7–10 October 2001; pp. 899–902.
51. Zhou, Q.; Lau, S.; Wu, D.; Shung, K.K. Piezoelectric films for high frequency ultrasonic transducers in biomedical applications. *Prog. Mater. Sci.* **2011**, *56*, 139–174.
52. Wang, Z.; Zhu, W.; Miao, J.; Zhu, H.; Chao, C.; Tan, O.K. Micromachined thick film piezoelectric ultrasonic transducer array. *Sens. Actuators A Phys.* **2006**, *130–131*, 485–490.
53. Sammoura, F.; Kim, S.-G. Theoretical modeling and equivalent electric circuit of a bimorph piezoelectric micromachined ultrasonic transducer. *IEEE Trans. Ultrason. Ferroelectr. Freq. Control* **2012**, *59*, 990–998.
54. Percin, G.; Khuri-Yakub, B.T. Piezoelectrically actuated flextensional micromachined ultrasound transducers. I. Theory. *IEEE Trans. Ultrason. Ferroelectr. Freq. Control* **2002**, *49*, 573–584.
55. Sammoura, F.; Smyth, K.; Kim, S.-G. Optimizing the electrode size of circular bimorph plates with different boundary conditions for maximum deflection of piezoelectric micromachined ultrasonic transducers. *Ultrasonics* **2013**, *53*, 328–334.
56. Jaffe, B.; Cook, W.R.; Jaffe, H.L. *Piezoelectric Ceramics*; Academic Press: Waltham, MA, USA, 1971; pp. 1–317.
57. Mo, J.-H.; Robinson, A.L.; Fitting, D.W.; Terry, F.L.; Carson, P.L. Micromachining for improvement of integrated ultrasonic transducer sensitivity. *IEEE Trans. Electron Devices* **1990**, *37*, 134–140.
58. Mo, J.H.; Fowlkes, J.B.; Robinson, A.L.; Carson, P.L. Crosstalk reduction with a micromachined diaphragm structure for integrated ultrasound transducer arrays. *IEEE Trans. Ultrason. Ferroelectr. Freq. Control* **1992**, *39*, 48–53.
59. Shelton, S.; Chan, M.-L.; Park, H.; Horsley, D.; Boser, B.; Izyumin, I.; Przybyla, R.; Frey, T.; Judy, M.; Nunan, K.; *et al.* CMOS-compatible AlN piezoelectric micromachined ultrasonic transducers. In Proceedings of 2009 IEEE International Ultrasonics Symposium, Rome, Italy, 19 – 23 September 2009; pp. 402–405.
60. Guedes, A.; Shelton, S.; Przybyla, R.; Izyumin, I.; Boser, B.; Horsley, D.A. Aluminum nitride pMUT based on a flexurally-suspended membrane. In Proceedings of 2011 16th International Solid-State Sensors, Actuators and Microsystems Conference, Beijing, China, 5–9 June 2011; pp. 2062–2065.
61. Percin, G.; Khuri-Yakub, B. Micromachined 2-D array piezoelectrically actuated flextensional transducers. In Proceedings of 1997 IEEE Ultrasonics Symposium Proceedings, Toronto, ON, Canada, 5–8 October 1997; pp. 959–962.

62. Suo, Z.; Hao, Z.; Qiao, D. The designing and manufacturing of 1 MHz piezoelectric micro-machined ultrasonic transducer. In Proceedings of 2012 Symposium on Piezoelectricity, Acoustic Waves, and Device Applications (SPAWDA), Shanghai, China, 23–25 November 2012; pp. 5–8.
63. Percin, G.; Khuri-Yakub, B.T. Piezoelectrically actuated flextensional MUTs. In Proceedings of 2001 IEEE Ultrasonics Symposium, Atlanta, GA, USA, 7–10 October 2001; pp. 903–906.
64. Perçin, G.; Khuri-Yakub, B.T. Piezoelectrically actuated flextensional micromachined ultrasound transducers. *Ultrasonics* **2002**, *40*, 441–448.
65. Hajati, A.; Latev, D.; Gardner, D.; Ottosson, M.; Imai, D.; Torrey, M.; Schoeppler, M. Monolithic ultrasonic integrated circuits based on micromachined semi-ellipsoidal piezoelectric domes. *Appl. Phys. Lett.* **2013**, *103*, 202906.
66. Muralt, P. PZT thin films for microsensors and actuators: Where do we stand? *IEEE Trans. Ultrason. Ferroelectr. Freq. Control* **2000**, *47*, 903–915.
67. Akai, D.; Yogi, T.; Kamja, I.; Numata, Y.; Ozaki, K.; Sawada, K.; Okada, N.; Higuchi, K.; Ishida, M. Miniature ultrasound acoustic imaging devices using 2-D pMUTs array on epitaxial PZT/SrRuO<sub>3</sub>/Pt/ $\gamma$ -Al<sub>2</sub>O<sub>3</sub>/Si structure. In Proceedings of 2011 16th International Solid-State Sensors, Actuators and Microsystems Conference, Beijing, China, 5–9 June 2011; pp. 910–913.
68. Mina, I.G.; Kim, H.; Kim, I.; Park, S.K.; Choi, K.; Jackson, T.N.; Tutwiler, R.L.; Trolier-McKinstry, S. High frequency piezoelectric MEMS ultrasound transducers. *IEEE Trans. Ultrason. Ferroelectr. Freq. Control* **2007**, *54*, 2422–2430.
69. Baborowski, J.; Ledermann, N.; Muralt, P. Piezoelectric micromachined transducers (PMUT's) based on PZT thin films. In Proceedings of 2002 IEEE Ultrasonics Symposium, Munich, Germany, 8–11 October 2002; Volume 2, pp. 1051–1054.
70. Jung, J.; Kim, S.; Lee, W.; Choi, H. Fabrication of a two-dimensional piezoelectric micromachined ultrasonic transducer array using a top-crossover-to-bottom structure and metal bridge connections. *J. Micromech. Microeng.* **2013**, *23*, 125037.
71. Yang, Y.; Tian, H.; Wang, Y.-F.; Shu, Y.; Zhou, C.-J.; Sun, H.; Zhang, C.-H.; Chen, H.; Ren, T.-L. An ultra-high element density pMUT array with low crosstalk for 3-D medical imaging. *Sensors* **2013**, *13*, 9624–9634.
72. Griggio, F.; Jesse, S.; Kumar, A.; Ovchinnikov, O.; Kim, H.; Jackson, T.N.; Damjanovic, D.; Kalinin, S.V.; Trolier-McKinstry, S. Substrate clamping effects on irreversible domain wall dynamics in lead zirconate titanate thin films. *Phys. Rev. Lett.* **2012**, *108*, 157604.
73. Baborowski, J.; Ledermann, N.; Muralt, P.; Schmitt, D. Simulation and characterization of piezoelectric micromachined ultrasonic transducers (PMUT's) based on PZT/SOI membranes. *Integr. Ferroelectr.* **2010**, *54*, 557–564.
74. Al-Hattamleh, O.; Cho, J. The effect of design and process parameters on electromechanical coupling for a thin-film PZT membrane. *J. Microelectromech. Syst.* **2006**, *15*, 1715–1725.
75. Yamashita, K.; Okuyama, M. Sensitivity improvement of diaphragm type ultrasonic sensors by complementary piezoelectric polarization. *Sens. Actuators A Phys.* **2006**, *127*, 119–122.
76. Dausch, D.E.; Gilchrist, K.H.; Castellucci, J.B.; Chou, D.R. Performance of flexure-mode pMUT 2D arrays. In Proceedings of 2007 IEEE Ultrasonics Symposium, New York, NY, USA, 28–31 October 2007; pp. 1053–1056.

77. Dausch, D.E.; Gilchrist, K.H.; Carlson, J.R.; Castellucci, J.B.; Chou, D.R.; von Ramm, O.T. Improved pulse-echo imaging performance for flexure-mode pMUT arrays. In Proceedings of 2010 IEEE International Ultrasonics Symposium, New York, NY, USA, 28–31 October 2010; pp. 451–454.
78. Percin, G.; Khuri-Yakub, B.T. Piezoelectrically actuated flextensional micromachined ultrasound transducers. II. Fabrication and experiments. *IEEE Trans. Ultrason. Ferroelectr. Freq. Control* **2002**, *49*, 585–595.
79. Ren, T.; Shu, Y.; Yang, Y.; Zhou, C.-J.; Wang, Y.; Tian, H.; Zhang, C.-H.; Sun, H.; Liu, X. Micromachined piezoelectric devices for acoustic applications. In Proceedings of 2012 IEEE International Conference on Electron Devices and Solid State Circuit (EDSSC), Bangkok, Thailand, 3–5 December 2012; pp. 1–4.
80. Fu, D.; Ren, T.; Chen, H.; Yang, Y.; Kong, X.; Ren, Y.; Liao, W.; Liu, L. A novel method for fabricating 2-D array piezoelectric micromachined ultrasonic transducers for medical imaging. In Proceedings of 2009 18th IEEE International Symposium on the Applications of Ferroelectrics, Xi'an, China, 23–27 August 2009; pp. 1–4.
81. Yamashita, K.; Chansomphou, L.; Murakami, H.; Okuyama, M. Ultrasonic micro array sensors using piezoelectric thin films and resonant frequency tuning. *Sens. Actuators A Phys.* **2004**, *114*, 147–153.
82. Wang, Z.; Zhu, W.; Zhu, H.; Miao, J.; Chao, C.; Zhao, C.; Tan, O.K. Fabrication and characterization of piezoelectric micromachined ultrasonic transducers with thick composite PZT films. *IEEE Trans. Ultrason. Ferroelectr. Freq. Control* **2005**, *52*, 2289–2297.
83. Mendoza-Lopez, J.; Sanchez-Lopez, C. Electromechanical Performance Comparison for Different Piezoelectric Micromachined Ultrasonic Transducer Element Geometries. In Proceedings of 2013 UKSim 15th International Conference on Computer Modelling and Simulation, Cambridge, UK, 10–12 April 2013; pp. 787–791.
84. Wang, Y.-F.; Ren, T.-L.; Yang, Y.; Chen, H.; Zhou, C.-J.; Wang, L.-G.; Liu, L.-T. High-density pMUT array for 3-D ultrasonic imaging based on reverse-bonding structure. In Proceedings of 2011 IEEE 24th International Conference on Micro Electro Mechanical Systems, Cancun, Mexico, 23–27 January 2011; pp. 1035–1038.
85. Wang, Y.-F.; Yang, Y.; Ren, T.-L.; Chen, H.; Liao, W.-J.; Kong, X.-M.; Wang, L.-G.; Zhou, C.-J.; Fu, D.; Liu, L.-T. Ultrasonic transducer array design for medical imaging based on MEMS technologies. In Proceedings of 2010 3rd International Conference on Biomedical Engineering and Informatics, Yantai, China, 16–18 October 2010; pp. 666–669.
86. MacLennan, D. Fundamental Characterisation and Early Functional Testing of Micromoulded Piezocomposites. Eng.D. Thesis, University of Strathclyde, Glasgow, UK, 2010, pp. 1–264.
87. Trolier-McKinstry, S.; Griggio, F.; Yaeger, C.; Jousse, P.; Zhao, D.; Bharadwaja, S.S.N.; Jackson, T.N.; Jesse, S.; Kalinin, S.V.; Wasa, K. Designing piezoelectric films for micro electromechanical systems. *IEEE Trans. Ultrason. Ferroelectr. Freq. Control* **2011**, *58*, 1782–1792.